Conf-950104--9

LBL-36243
UC-1600

Lawrence Berkeley Laboratory

UNIVERSITY OF CALIFORNIA

ENERGY & ENVIRONMENT DIVISION

Presented at the ASHRAE Symposium, Chicago, IL, Jan. 28–Feb. 1, 1995, and to be published in ASHRAE Transactions 101(1) (1995)

Measurement of Bidirectional Optical Properties of Complex Shading Devices

J.H. Klems and J.L. Warner

January 1995

ENERGY
AND ENVIRONMENT
DIVISION

Prepared for the U.S. Department of Energy under Contract Number DE-AC03-76SF00098

DISCLAIMER

This document was prepared as an account of work sponsored by the United States Government. While this document is believed to contain correct information, neither the United States Government nor any agency thereof, nor The Regents of the University of California, nor any of their employees, makes any warranty, express or implied, or assumes any legal responsibility for the accuracy, completeness, or usefulness of any information, apparatus, product, or process disclosed, or represents that its use would not infringe privately owned rights. Reference herein to any specific commercial product, process, or service by its trade name, trademark, manufacturer, or otherwise, does not necessarily constitute or imply its endorsement, recommendation, or favoring by the United States Government or any agency thereof, or The Regents of the University of California. The views and opinions of authors expressed herein do not necessarily state or reflect those of the United States Government or any agency thereof, or The Regents of the University of California.

Lawrence Berkeley Laboratory is an equal opportunity employer.

DISCLAIMER

Portions of this document may be illegible in electronic image products. Images are produced from the best available original document.

LBL-36243
DA-330

ASHRAE Transactions 101(1) (1995).

MEASUREMENT OF BIDIRECTIONAL OPTICAL PROPERTIES OF COMPLEX SHADING DEVICES

J. H. Klems and J. L. Warner
Building Technologies Program
Energy and Environment Division
Lawrence Berkeley Laboratory
University of California
Berkeley, CA 94720

January 1995

This work was supported by the Assistant Secretary for Energy Efficiency and Renewable Energy, Office of Building Technologies, Building Systems and Materials Division of the U.S. Department of Energy under Contract No. DE-AC03-76SF00098.

DISTRIBUTION OF THIS DOCUMENT IS UNLIMITED

MASTER

MEASUREMENT OF BIDIRECTIONAL OPTICAL PROPERTIES OF COMPLEX SHADING DEVICES

J. H. Klems and J. L. Warner

Building Technologies Program

Lawrence Berkeley Laboratory

Berkeley, CA 94720

Abstract

A new method of predicting the solar heat gain through complex fenestration systems involving nonspecular layers such as shades or blinds has been examined in a project jointly sponsored by ASHRAE and DOE. In this method, a scanning radiometer is used to measure the bidirectional radiative transmittance and reflectance of each layer of a fenestration system. The properties of systems containing these layers are then built up computationally from the measured layer properties using a transmission/multiple-reflection calculation. The calculation produces the total directional-hemispherical transmittance of the fenestration system and the layer-by-layer absorptances. These properties are in turn combined with layer-specific measurements of the inward-flowing fractions of absorbed solar energy to produce the overall solar heat gain coefficient.

This paper describes the method of measuring the spatially averaged bidirectional optical properties using an automated, large-sample gonio-radiometer/photometer, termed a "Scanning Radiometer." Property measurements are presented for one of the most optically complex systems in common use, a venetian blind. These measurements will form the basis for optical system calculations used to test the method of determining performance.

INTRODUCTION

The recent effort of the National Fenestration Rating Council (NFRC), a voluntary association of fenestration product manufacturers, to establish product ratings for U-value and solar heat gain coefficient (and, ultimately, for energy performance) has given new currency to issues of long-standing interest to ASHRAE. In the case of solar heat gain coefficient, geometrically or optically complicated shading systems can (in fact, are intended to) have a major impact on performance; this situation is in sharp contrast to that of U-values, where, except in special cases, shading or add-on devices play a minor role compared to the intrinsic properties of the window unit. Frequently shading systems are add-on interior or exterior devices ("attachments"), although sometimes they are integral parts of the window unit (e.g., between-pane blinds). In all cases the problem of determining the solar heat gain coefficient—which is a *system* property depending on

This research was jointly supported by ASHRAE, as Research Project 548-RP under Agreement No. BG 87-127 with the U.S. Department of Energy, and by the Assistant Secretary for Energy Efficiency and Renewable Energy, Office of Building Technologies, Building Systems and Materials Division of the U.S. Department of Energy under Contract No. DE-AC03-76SF00098.

all the elements in the fenestration—is complicated by the "combinatorial problem": a single shading device may be combined with glazing systems having various numbers of glazing layers of differing thicknesses, coatings and tints to produce a dazzling number of possible combinations. Even clear glazing layers have solar-optical absorptances and reflectances that, while small, are not negligible at (near-) normal incidence, and these increase significantly at high incident angles, where much summer sunlight and diffuse daylight in fact occur, so that it is not possible to neglect these "combinatorial" effects out of hand. To make matters worse, color and solar-optical reflectance are closely related, and color is an important architectural variable: some shading systems may be offered in a large number of colors and patterns. In sum, these considerations make the prospect of determining solar heat gain coefficients primarily by the traditional method of system-level calorimeter measurements, which are time-consuming, economically unattractive.

The solar-optical transmittance of a fenestration system is always an important part of the solar heat gain coefficient, and in many cases is the dominant one. Solar-optical effects are in many ways simpler to deal with, both theoretically and experimentally, than are calorimetric. The specifically calorimetric effects in the solar heat gain coefficient deal with the motion of absorbed radiant energy through the fenestration system as heat, and are independent of differences in color (unless they are associated with differences in emissivity). Thus, for many of the combinations having different solar heat gain coefficient, the specifically calorimetric effects will be the same. For this reason, it is worthwhile to explore the extent to which solar heat gain coefficients can be determined through separate determinations of the relevant solar-optical and calorimetric properties, and, further, whether the combinatorial problem can be alleviated by separately determining the solar-optical properties of individual subsystems (or "layers") and combining them by calculation into system properties. (Papamichael, Klems, & Selkowitz, 1988; Papamichael & Winkelmann, 1986)

These issues are being explored in a research project sponsored jointly by ASHRAE and the U.S. Department of Energy, and a method of deriving solar heat gain coefficients from separate solar-optical measurements on layers and calorimetric measurements on representative systems has been developed, and preliminary results showing the feasibility of the scheme have been presented (Klems & Warner, 1992). Two prior publications, denoted Paper 1 (Klems, 1994A) and Paper 2 (Klems, 1994B), have described the physical basis of the method and the mathematical method of calculating the solar heat gain coefficient from the bidirectional* optical properties of individual layers (e.g., shading devices) in the fenestration system. This paper describes the method of measuring complex shading devices and deriving these layer bidirectional properties. Planned future publications will discuss the determination of the calorimetric properties (i.e., inward-flowing fractions) and empirical tests of the resulting solar heat gain coefficients calculated.

The layer measurements described here can also be utilized to produce a detailed and accurate calculation of the daylight provided by a fenestration system (Papamichael, 1990), a subject that is outside the scope of the current work.

---

* Since bidirectional properties are defined for infinitesimally small incident and outgoing solid angle intervals, any measurement of course produces biconical quantities measured over finite solid angles. These solid angles are presumed to be small enough (or the properties sufficiently slowly varying) that the properties measured over the small finite solid angles used are a good approximation to the bidirectional properties.

MEASUREMENT OF BIDIRECTIONAL OPTICAL PROPERTIES

It was necessary to develop an apparatus capable of measuring the bidirectional transmittance and reflectance distribution of a sample of dimensions large enough to provide a reasonable average over periodic device features such as blind slats. Ideally, one would have liked to use a sample on the order of a full window size, 1 m^2. Unfortunately, this would have made the apparatus prohibitively large and expensive. We settled for a design sample size of 10 in. square, and ended with a usable sample size of 7.5 in. square.

We constructed a large-sample, automated gonio-radiometer/photometer ("scanning radiometer"), shown in Figures 1 and 2. In this apparatus a calibrated detector measures the outgoing radiation at a large number of angular positions distributed over either the front or rear outgoing hemisphere, and this measurement is repeated for all combinations of incident angles that it is necessary to sample, depending on the inherent symmetry of the layer under test. Bidirectional transmittance and reflectance are determined from these measurements and the measured incident irradiance. Radiometric (350-2200 nm) and photometric data are recorded simultaneously. This apparatus has been variously denoted a "scanning radiometer," an "automated scanner," and a "bidirectional scanner," depending on which of its features was being emphasized; for brevity we refer to it here as the "scanner."

The detector optical system is shown in Figure 3, with an explanation of its operation in Figure 4. Radiation within a narrow angular cone around the detector axis is focused on the entrance port of an integrating sphere that contains the radiometric and photometric sensors. The collection system is characterized by high demagnification and high angular dispersion. Light collection is insensitive to position within the sample plane until the cone of angular acceptance originating at a point in the sample plane begins to clip the edge of the collection mirror. It is this effect that limits the size of the usable sample.

Measurements are made in an apparatus coordinate system (x_A, y_A, z), which is related to the space coordinate systems used in Paper 1 and Paper 2 as shown in Figure 5.

As currently configured, the scanner proceeds through the following measurement sequence. The sample plane begins with $\theta=0$ and $\phi=0$ (see Figures 1 and 5). The detector arm moves to an initial position with $\gamma=-90^\circ$ and $\beta=-70.5^\circ$ (which is the limit of vertical travel possible for the detector due to the size of the collection mirror). The detector then begins to move continuously up the semicircular detector arm, with data recorded each 1.5° of travel in β. (For historical reasons, data collection includes scans at $\gamma=\pm 90^\circ$, although because the mirror views both sides of the sample plane this data is meaningless and is discarded.) Light source monitor readings are recorded at the beginning, middle (the detector pauses at the center of its arc) and end of each vertical scan. When the detector reaches the end of its vertical travel ($\beta=+70.5^\circ$) the detector arm advances to increase γ by 15° and the vertical motion of the detector recommences in the opposite direction. This sequence of events repeats until the entire outgoing hemisphere has been sampled from -75° to 75° at 15° intervals in γ and from -70.5° to 70.5° at 1.5° intervals in β. (Note that the outgoing hemisphere is defined relative to the sample plane.) This entire sequence, comprising the outgoing hemisphere scan, requires about 20 minutes to complete. Next, the sample plane automatically rotates around the vertical axis to increase θ by 15°, and the detector and detector arm return to their starting positions relative to the sample plane, and the outgoing hemisphere scan

repeats. A total of six incident angle (θ) measurements are made, 0-75º at 15º intervals. If the sample is not azimuthally symmetric, or if more measurements are needed, the scanner next rotates the sample by 15º in its plane (ϕ) and the entire sequence of incident angle steps and outgoing hemisphere scans is repeated. In this manner measurements are accumulated over a four-dimensional grid of $\{\gamma, \beta, \theta, \phi\}$. Reflectance measurements are made with the same set of scanner motions, except that initially the entire sample-plane-detector-arm assembly is rotated around the vertical axis by 180º and the sample repositioned as required. On a device without front-back symmetry, four measurement sequences would normally be carried out: front transmission, back transmission, front reflection and back reflection. We do not normally use the relation between front and back bidirectional transmittance to reduce the number of measurements made.

For an outgoing radiance of $I(\theta, \phi)$ from the sample, the rate, W, at which energy enters the detector aperture is given by

$$W(\theta,\phi) = I(\theta,\phi) \cdot \mathbf{A}_S \cdot \cos(\theta) \cdot \Omega_D, \tag{1}$$

where $\mathbf{A}_S$ is the sample area and Ω_D is the (small) solid angle subtended by the detector aperture (the aperture of the integrating sphere) as seen from the sample. The notation used here is that of Paper 1 and Paper 2. This energy flow produces an output signal from the sensor on the integrating sphere (termed the "probe" signal) of

$$V = \mathbf{G} \cdot (k\varepsilon) \cdot I(\theta, \phi) \cdot \mathbf{A}_S \cos(\theta) \cdot \Omega_D, \tag{2}$$

where $\mathbf{G}$ is the amplifier gain (see Figure 6) and the constant ($k\varepsilon$) is the effective detector response, consisting of combined effects of the mirror reflectance and sphere efficiency (ε) and the detector sensitivity (k). The combination ($k\varepsilon$) can be considered as the output voltage per unit of energy directed into the detector aperture. With this definition, Ω_D is a purely geometric quantity. It was determined by a Monte Carlo simulation (Hammersley & Handscome, 1964) . From the definition of transmittance and reflectance distribution functions in Equations 1.4, the transmittance of a sample may be determined from the measurement by

$$\tau(\theta, \phi; \theta_S, \phi_S) = \frac{I(\theta, \phi)}{E(\theta_S, \phi_S)} = \frac{V(\theta, \phi)}{E(\theta_S, \phi_S) \cdot \mathbf{G} \cdot (k\varepsilon) \cdot \mathbf{A}_S \cos(\theta) \cdot \Omega_D}, \tag{3a}$$

and when the scanner probe is swung around to measure reflectance from the front side of the sample the corresponding equation is used to determine reflectance:

$$\rho(\theta^r, \phi^r; \theta_S, \phi_S) = \frac{J(\theta^r, \phi^r)}{E(\theta_S, \phi_S)} = \frac{V(\theta^r, \phi^r)}{E(\theta_S, \phi_S) \cdot \mathbf{G} \cdot (k\varepsilon) \cdot \mathbf{A}_S \cos(\theta) \cdot \Omega_D}. \tag{3b}$$

Calibration of the scanner consists in determining ($k\varepsilon$) and $E(\theta_S, \phi_S)$. Since neither of these depends on the position of the scanner probe, the apparatus can be calibrated in the transmission mode. This is done by first establishing the relation between the sample plane incident irradiance and the source monitor, $\mathbf{S}$, which is a radiometric detector viewing the source from a fixed location. This relationship is linear for the operating voltage region of the source lamp and the

normal-incidence irradiance, E_0, is calculated from S by the equation $E_0 = \mu \cdot S$, where μ is a constant determined by a separate calibration procedure that consists of inserting the calibration sensor indicated in Figure 6 at the sample plane and measuring E_0 and S for varying source intensity settings. Since the source is axially symmetric, the incident irradiance for other incident directions is given by

$$E(\theta_s, \phi_s) = E_0 \cos(\theta_s). \tag{4}$$

The constant ($k\varepsilon$) was measured by setting the probe direction on the system axis (the origin of the coordinate system) and viewing the source through a small (area A_C, 2 in X 2 in) aperture placed at normal incidence (for technical reasons this was actually accomplished in four measurements using a 1 in X 1 in aperture). This is effectively measurement of a (small) specular sample of transmission one. For such a specular sample the combination of Equation 2 with Equation 4 must be modified to read

$$\frac{U}{E_0 \cdot A_C} = \frac{G \cdot (k\varepsilon) \cdot \tau_{sp} \cdot \Omega_{DS}}{\Omega_{SS}} \frac{\langle (AI)_S \rangle_C}{\langle (AI)_S \rangle_S} \equiv \mathcal{A}_{sp} \cdot G \cdot (k\varepsilon) \cdot \tau_{sp}, \tag{5}$$

where the quantity $(AI)_S$ is the source illuminance-area product, the bracketed quantity in the denominator indicates an average over all parts of the source visible from the sample, while the quantity in the numerator indicates an average only over those parts of the source visible to the detector through the aperture C (which could be the size of a specular sample). The quantity Ω_{SS} is the solid angle subtended by the sample as seen from the source, while Ω_{DS} is the solid angle of the detector aperture as seen from the source. The right-hand expression serves to define the effective specular acceptance, $\mathcal{A}_{sp}$, which collects these four quantities. This acceptance was evaluated by Monte Carlo calculation, assuming a uniform source luminance, and found to be $\mathcal{A}_{sp} = 0.90 \pm 0.04$ for the calibration. Knowing this and with an open aperture as a source ($\tau_{sp} = 1$), the measurement determines the constant ($k\varepsilon$), which is about 2.2 V/W. It must be redetermined if any element of the source/sample/source-monitor geometry is changed.

In practice, there were also variations in the measurement geometry that affect the interpretation of the results. The simple geometry, shown in Figure 7(A), used to measure thin samples such as shades, contained apertures that shadowed the sample edges for measurements at large angle (either incident or outgoing). For thick samples such as venetian blinds, it was necessary to modify the geometry considerably to reduce such shadowing, resulting in the geometry of Figure 7(B). The effect of the sample geometry is to reduce somewhat the radiation arriving at the detector by obstructing the view of the detector for certain configurations. This reduction is purely geometrical, but depends on the sample and detector positioning in a complex way. It is accounted for by defining another effective acceptance, $\mathcal{A}_{eff}$, the fraction of the total sample area visible to the detector for a given measurement configuration. It is inserted into Equations 3 to produce the final equations for deriving nonspecular sample properties from the measurements:

$$\tau(\theta,\phi;\theta_S,\phi_S) = \frac{V(\theta,\phi)}{\mathbf{E}_0 \cos(\theta_S)\cdot \mathbf{G}\cdot(k\varepsilon)\cdot \mathbf{A}_S \cos(\theta)\cdot \Omega_D \cdot \mathcal{A}_{eff}(\gamma,\beta;\theta_S,\phi_{SAM})} \qquad (6a)$$

$$\rho(\theta^r,\phi^r;\theta_S,\phi_S) = \frac{V(\theta,\phi)}{\mathbf{E}_0 \cdot (k\varepsilon)\cdot \mathbf{G}\cdot \mathbf{A}_S \cos(\theta_S)\cos(\theta)\cdot \Omega_D \cdot \mathcal{A}^r_{eff}(\gamma,\beta;\theta^r_S,\phi_{SAM})}, \qquad (6b)$$

where the effective acceptances $\mathcal{A}_{eff}$ and $\mathcal{A}^r_{eff}$ depend explicitly on the experimental variables in Figure 5, as indicated. Measurements established that the combination $\mathbf{E}_0 \cdot (k\varepsilon)$ is constant to within 10% over the sample area, which is a check both for uniformity of sample irradiation and spatial variations in the mirror reflectance.

The apparatus was first calibrated with open-sample-port transmission measurements, and later using a 7.5 in. square Spectralon® lambertian reflector of known (approximately 98%) hemispherical reflectance, uniform with wavelength over the 350-2200 nm region. The two calibration procedures agreed to within 1% for moderate angles, assuming $\mathcal{A}_{eff}$=1, and the calibrated-reflector measurements using the photometric sensor were used to determine the effective acceptance at larger angles, where $\mathcal{A}_{eff}$ was expected to become significantly different from one. These measurements produced results like those shown in Figure 8, and yielded all the information necessary for determining transmittance for all types of samples. For thick samples in reflectance the acceptance determination was less accurate than for thin samples or for thick samples in transmittance, and for both types of samples accuracy is considerably poorer at the largest incident angles.

The acceptances determined in this way were then checked using the radiometric measurements on the Spectralon® sample. The layer analysis software was used to integrate the measured outgoing distributions, producing measured directional-hemispherical reflectances. The measurements were made over a set of incident angles and azimuths, as would be done for a bilaterally symmetric device such as a venetian blind. Since the calibration sample is azimuthally symmetric, the apparent variation of the measurements with azimuth angle gave an estimate of the experimental uncertainty. The results of these measurements are plotted in Figure 9. The measured hemispherical reflectances are consistent within their experimental error with the 99% reflectance of the calibration sample. Measurements become very inaccurate (±40%) at the largest incident angle (75º) but are still reasonably accurate (±10%) at 60º incidence. Part of the uncertainty at 75º incidence comes from surround reflectance and affects only reflectance measurements; however, uncertainties in the geometric acceptance at this angle remain substantial.

We next measured the shading devices used in the systems under study. Measurements on the white translucent shade were utilized to determine the directional-hemispherical properties shown in Figure 10. Derived by integrating measurements of the complete outgoing distribution and determining absorptance from the measured transmittance and reflectance, these measurements confirm the assumptions of our previous publication (Klems & Warner, 1992) on this system, which assumed diffuse behavior at large outgoing angles. These measurements show a small difference between the photometric and radiometric properties of the shade; however, because the radiometric signal is quite small we consider the differences to be unreliable due potential uncertainties in background subtraction and thermal drift. These are not well known yet and are not included in the estimated errors.

Figure 11 illustrates the transmittance properties of a white venetian blind. This figure is drawn from a set of measurements made on the blind with the slats at a 45º tilt; data were also accumulated for the slats fully closed and fully open (horizontal). Each set of measurements included bidirectional measurements over the full range of incident and outgoing directions for both reflection and transmission, front and back incidence. Where possible, symmetries were utilized to reduce the number of measurements that needed to be made (e.g., since the blinds are right-left symmetric, it was only necessary to measure over a range of 180º in the incident azimuth, rather than 360º). The full outgoing hemisphere was measured for each incident condition, as described above.

In Figure 11 the upper plot (A) presents the directional-hemispherical transmittance as a function of incident direction, while the lower plot (B) gives the transmittance distribution function τ as a function of the outgoing angles in the scanner measurement coordinate system. Each point in the plot (A) results from integrating over a plot such as the one shown in (B). The particular incident direction corresponding to plot (B) is indicated by the arrow in (A), and corresponds to the measurement configuration shown in Figure 12. If we visualize the venetian blind as mounted in a window in the xy plane with the yz plane horizontal and the zx plane vertical and perpendicular to the window, then the figure corresponds to a physical situation in which the sun is at an altitude of 45º and in the plane perpendicular to the window. The angle β then runs along the slats, while γ is the vertical angle of the transmitted radiation, with negative γ denoting downward-going radiation.

The strongly asymmetric character of 11A is thus understandable as the result of the downward blind tilt, which in our example excludes the direct sun, but is highly transmitting for upward-going radiation, which would arise from ground reflection. The outgoing transmittance distribution in 11B (corresponding, in our example, to transmittance for direct sunlight) thus shows a minimum at the direct sun angle (γ=-45º), a broad ridge at around γ=0, which is radiation twice diffusely reflected from the blind slats, and a higher broad ridge at large positive γ, which is radiation once diffusely reflected from the front side of the blind. More detailed information on the transmittance for downward-going radiation is given in Figure 13, which shows that for moderate outgoing angles the rectilinear geometry of the blind slats is reflected in the transmission distribution, while the small transmission at very large outgoing angles appears to be more uniform. One would expect this if the transmission at large angles arises from multiple diffuse reflection from several blind slats.

We see from this example the large amount of information necessary to characterize a system as complex as a venetian blind at a single slat tilt. To put this into perspective, a sun-following calorimeter measurement, if successful, might take (in an optimistic estimate) on the order of half a day, and would give a single point in 11A. On the scanner this measurement takes around 20 minutes, yields around one thousand data points, and enables us to construct 11B. In either case, in order to characterize accurately the blind heat gain (for a given slat angle) including beam, diffuse and ground-reflected radiation, one would need all of the information in 11A, which contains some 78 directional-hemispherical measurements, a lengthy measurement with the scanner, but a much more arduous one with a calorimeter (i.e., at least 12 times slower). In fact, the situation for calorimeter measurement is worse than this indicates, since many of the incident angle configurations would be either unobtainable or exceedingly hard to obtain with a calorimeter measurement. (Operational constraints differ for indoor and outdoor calorimeters, but in either case it is true that there is less measurement flexibility than for a purely solar-optical measurement.)

The additional detail of 11B provided by the scanner measurement is the information that allows one to carry out a layer calculation, as opposed to making separate measurements for each fenestration combination containing the blind.

DISCUSSION

The small differences between radiometric and photometric hemispherical properties of the white shade for small (≤30º) incident angles do suggest a spectral dependence of the optical properties, although our present radiometric measurements are not reliable enough to permit a separate radiometric analysis. Above 30º the apparent rise in radiometric reflectance (which is mirrored in the fall of the derived absorptance to unphysical negative values) is a measurement artifact probably due to a combination of a small signal-to-noise ratio and a significant surround reflectance.

For the blind measurements even worse problems with the radiometric data were apparent from detailed study of the data. Whenever the blind allowed direct transmission of the incident radiation, there was a consequent heating of the detector integrating sphere that biased the radiometric sensor measurement for a large and variable recovery period. This made the radiometric data essentially unusable for this type of sample. The fact that the scanner radiometric data did not prove reliable for these measurements is disappointing, but simply indicates the necessity of continued improvements in the instrumentation. The reason for the problem is well understood and can be addressed, as can other apparatus and methodological problems identified during the project. It should not be taken as an indictment of the general method of determining solar heat gain coefficient.

CONCLUSIONS

We have demonstrated that it is possible to make the detailed measurements of bidirectional, spatially averaged optical properties necessary to characterize a complex optical layer such as a venetian blind or other shading device, which is both optically nonspecular and, while periodic, spatially non-homogeneous on the scale over which optical characterizations are usually made.

While the data set characterizing these properties is voluminous, measurement rates still compare favorably to utilizing a calorimeter to measure the same optical properties (i.e., at least 12 times faster). A great deal of the data accumulated is necessary for generating system properties from layer measurements, so that all combinations of different fenestration elements do not need separate measurement. Much faster measurement methods (such as an integrating sphere) could be utilized at the cost of needing to measure complete systems rather than (or possibly in addition to) individual layers.

Issues of spectral properties, both differences between visible and near-infrared optical properties and correlations between spectral and angular property variations (for example, increasing differences between visible and near-infrared properties at larger angles) remain to be investigated.

ACKNOWLEDGMENTS

The authors are grateful for the efforts of Konstantinos Papamichael, who was active in a number of areas in the initial stage of this work, including early work on calibrating the scanning

radiometer and writing the first version of the computer code that calculates hemispherical properties from the angular distribution, of R. Muthukumar, who later updated and extended the compute code, and of Mark Spitzglas, who participated in the early stages of scanning radiometer design and construction. The efforts of Dennis DiBartolomeo, Mary Hinman, Jonathan Slack, and Mehrangiz Yazdanian were vital to the completion and automation of the scanning radiometer, and the further efforts of Dennis DiBartolomeo and Jonathan Slack in maintaining and improving its operation during the course of these measurements were critical.

This research was jointly supported by ASHRAE, as Research Project 548-RP under Agreement No. BG 87-127 with the U.S. Department of Energy, and by the Assistant Secretary for Conservation and Renewable Energy, Office of Building Technologies, Building Systems and Materials Division of the U.S. Department of Energy under Contract No. DE-AC03-76SF00098.

REFERENCES

Hammersley, J. M., & Handscome, D. C. (1964). Monte Carlo Methods. London: Methuen.

Klems, J. H. (1994A). A New Method for Predicting the Solar Heat Gain of Complex Fenestration Systems: I. Overview and Derivation of the Matrix Layer Calculation. ASHRAE Trans., 100(pt. 1).

Klems, J. H. (1994B). A New Method for Predicting the Solar Heat Gain of Complex Fenestration Systems: II. Detailed Description of the Matrix Layer Calculation. ASHRAE Trans., 100(pt.1).

Klems, J. H., & Warner, J. L. (1992). A New Method for Predicting the Solar Heat Gain of Complex Fenestration Systems. In Thermal Performance of the Exterior Envelopes of Buildings V, (pp. 303-312). Clearwater Beach, FL: American Society of Heating, Refrigerating and Air-Conditioning Engineers, Inc.

Papamichael, K. (1990). Fenestrations as Luminaires of Varying Candlepower Distribution. In IEEE Industry Applications Society Conference, Seattle, WA: IEEE.

Papamichael, K., Klems, J., & Selkowitz, S. (1988). Determination and Application of Bidirectional Solar-Optical Properties of Fenestration Systems. In 13th National Passive Solar Conference, Cambridge, MA.

Papamichael, K., & Winkelmann, F. (1986). Solar-Optical Properties of Multilayer Fenestration Systems. In International Daylighting Conference, II, Long Beach, CA.

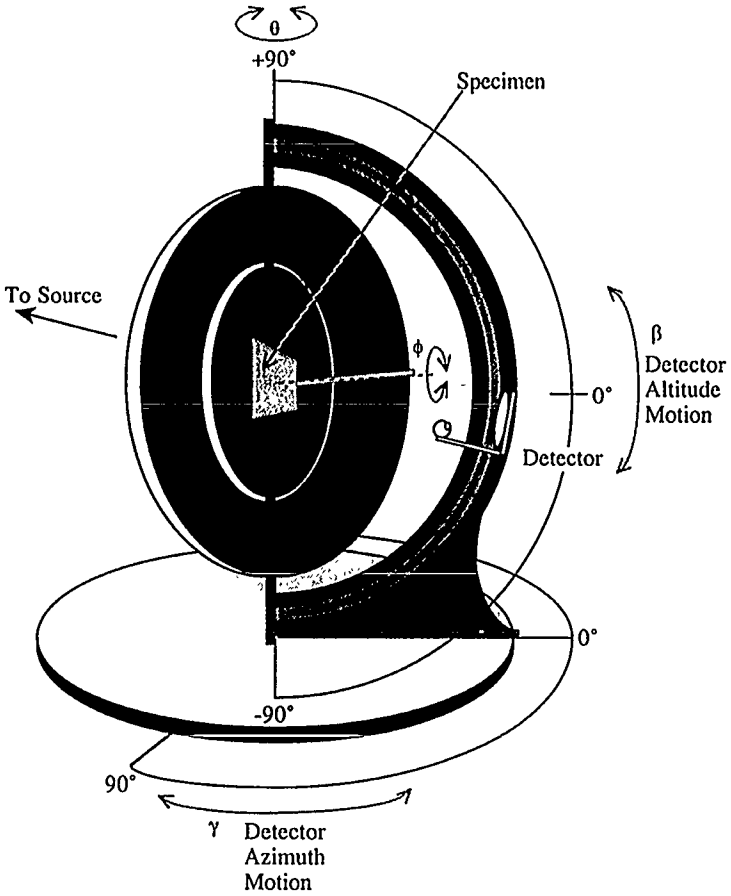

Fig 1. A Schematic Drawing of the Scanning Radiometer. The apparatus consists of a fixed source and a sample mounted on a plane that rotates about a fixed vertical axis relative to the source, to produce a given incident angle, θ. The sample also rotates about an axis perpendicular to this plane to produce the incident azimuthal angle, ϕ. The detector is mounted on a semicircular arm that rotates through the probe azimuth angle, γ, about a vertical axis through the center of the sample. The detector moves up and down over this semicircular arm to vary the probe altitude angle, β, producing an angular coverage over the entire outgoing hemisphere relative to the sample.

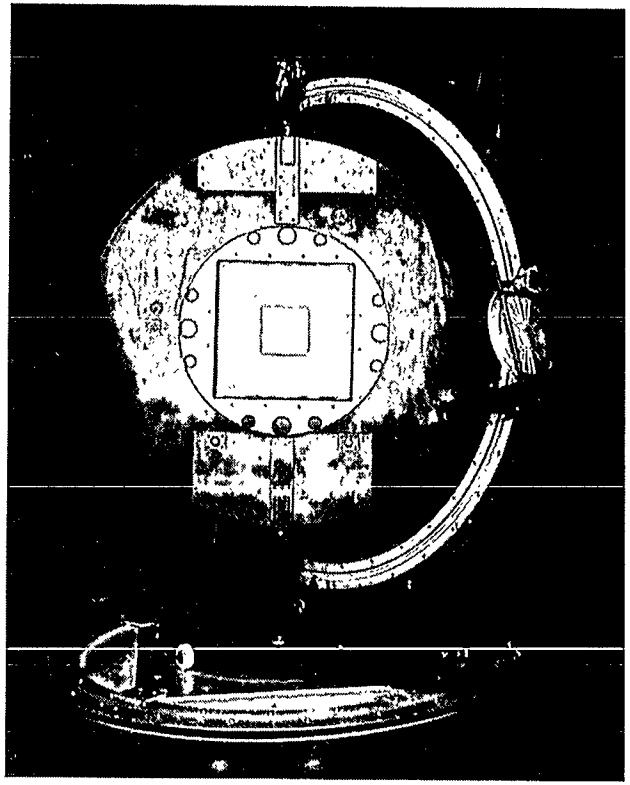

CBB 900 8295

Fig 2. A photograph of the Scanning Radiometer. The detector arm is in the forward-hemisphere-scanning configuration used to measure bidirectional reflectance.

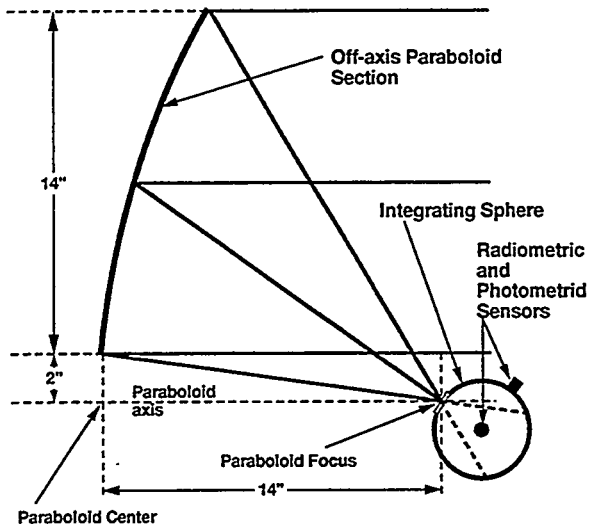

Fig 3. Scanner Detector Optical Collection System. The detector consists of a collecting mirror, and integrating sphere, and a pair of sensors. Light parallel to the axis of the detection system is collected by an off-axis parabolic mirror and focused onto the entrance point of an integrating sphere containing both radiometric and photometric sensors. This scheme provides wavelength-independent collection of radiation from a large sample area combined with a sharp angular selectivity. Radiometric and photometric data are recorded simultaneously. The radiometric sensor has a flat spectral response, and wavelength sensitivity is determined by the reflectance characteristics of the integrating sphere coating, which is good from 350-2200 nm.

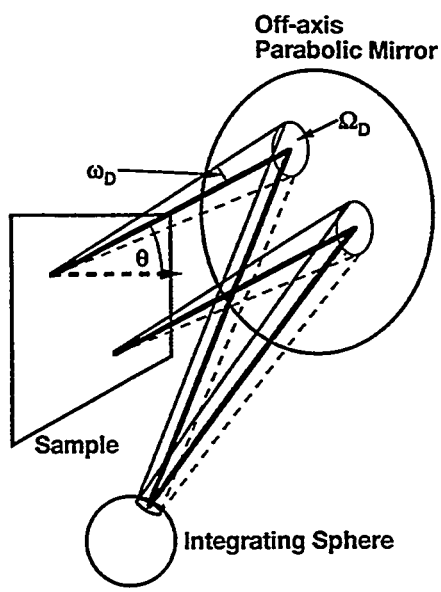

Fig 4. Operation of the Scanner Optical Collection System. For a detector outgoing direction θ parallel rays in that direction from different points in the sample plane (heavy lines), which lie along the detector optical axis, strike the collection mirror and are focused onto the center of the integrating sphere aperture. Corresponding rays lying off-axis by an angle ω_D (light solid lines) are focused to a point on the edge of the integrating sphere aperture. A different set of corresponding rays (dashed lines) deviating by the same angle from the central ray will be focused onto a different point on the edge of the aperture. All rays with an angular deviation from the central ray less than ω_D will go into the integrating sphere aperture. This defines a solid angle cone of acceptance Ω_D of opening half-angle ω_D. Collection of radiation will be the same for all points in the sample plane until the solid angle acceptance cone intersects the mirror edge, which defines the maximum possible sample size.

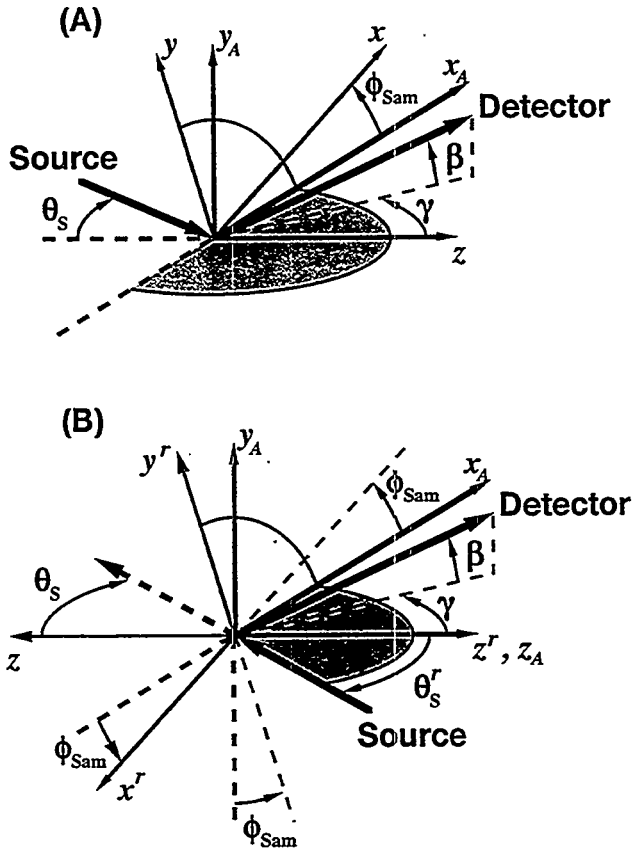

Fig 5. Scanner Apparatus Coordinate Systems. The detector position is specified by an azimuthal angle γ and an altitude angle β relative to a coordinate system x_A y_A z that is fixed in the sample plane. This coordinate system is right-handed, y_A points upward, and z is normal to the sample plane pointing into the detection hemisphere. (A) Transmission coordinate system. The source polar angle θ_S is set by rotating the sample plane relative to the source, while the source azimuth is obtained by rotating the sample in its plane by an angle ϕ_{Sam} equal to the negative of the suplement of the desired source azimuth. The relationship between the apparatus coordinate system and the layer transmission coordinate system x y z is shown. (B) Reflection coordinate system. For reflectance measurements the entire sample plane and detector hemisphere is rotated around a vertical axis by 180°. The source polar angle θ_S is again obtained by rotating the sample plane. Since the sample is rotated in its plane in the same sense relative to the detection coordinate system, ϕ_{Sam} will now be equal to the negative of the source azimuth. The relationship between the apparatus coordinate system and the layer backward-hemisphere coordinate system x^r y^r z^r is shown. Note that the latter is a left-handed system. The apparatus and appropriate layer z axes (i.e., z for transmission, z^r for reflection) coincide.

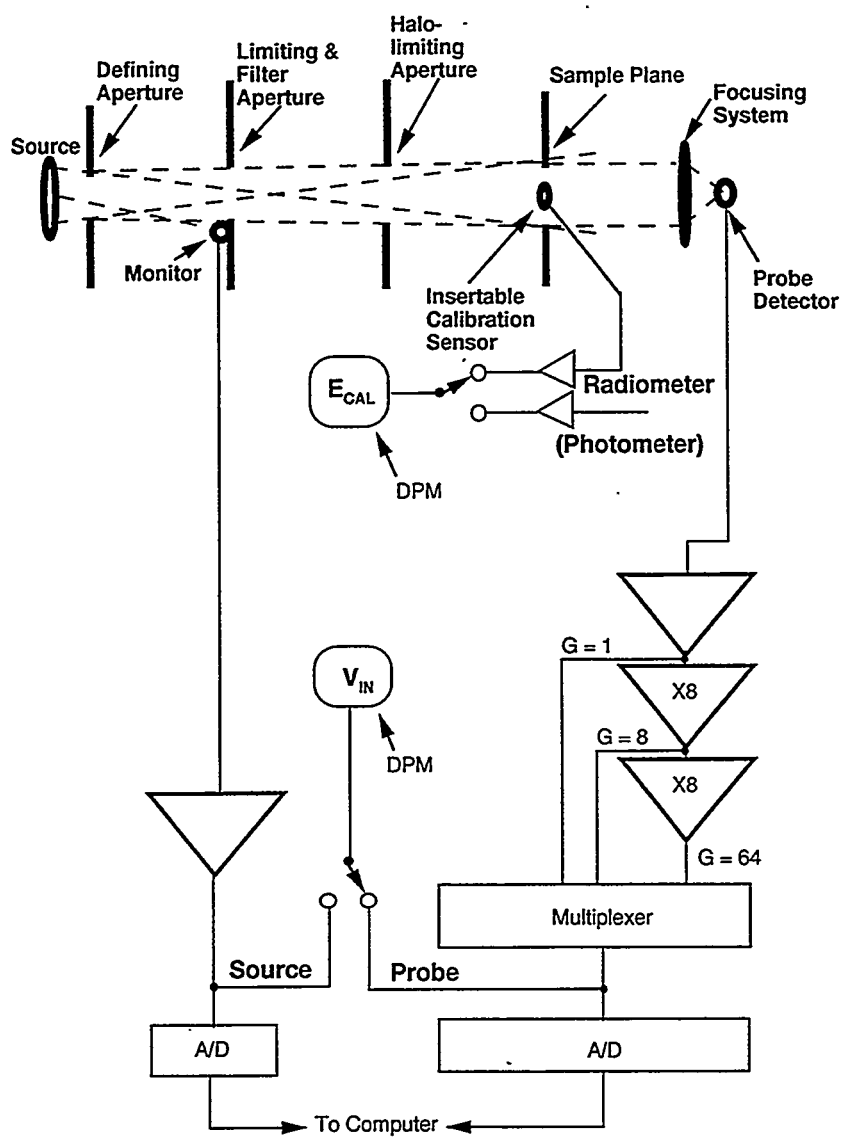

Fig. 6. Schematic Diagram of the Scanner Data Collection System. The probe signal is amplified by three cascaded amplifiers with the output of each sent to the computer through a multiplexer and digitizer to produce a computer-selectable gain for the probe signal, which has a large potential dynamic range. Signals from the G=1 output are used in calibration. A removable radiometer at the sample plane is used in calibration to relate the sample plane incident irradiance to the signal from the source monitor. Calibration data is recorded manually through display on a digital panel meter (DPM) as indicated.

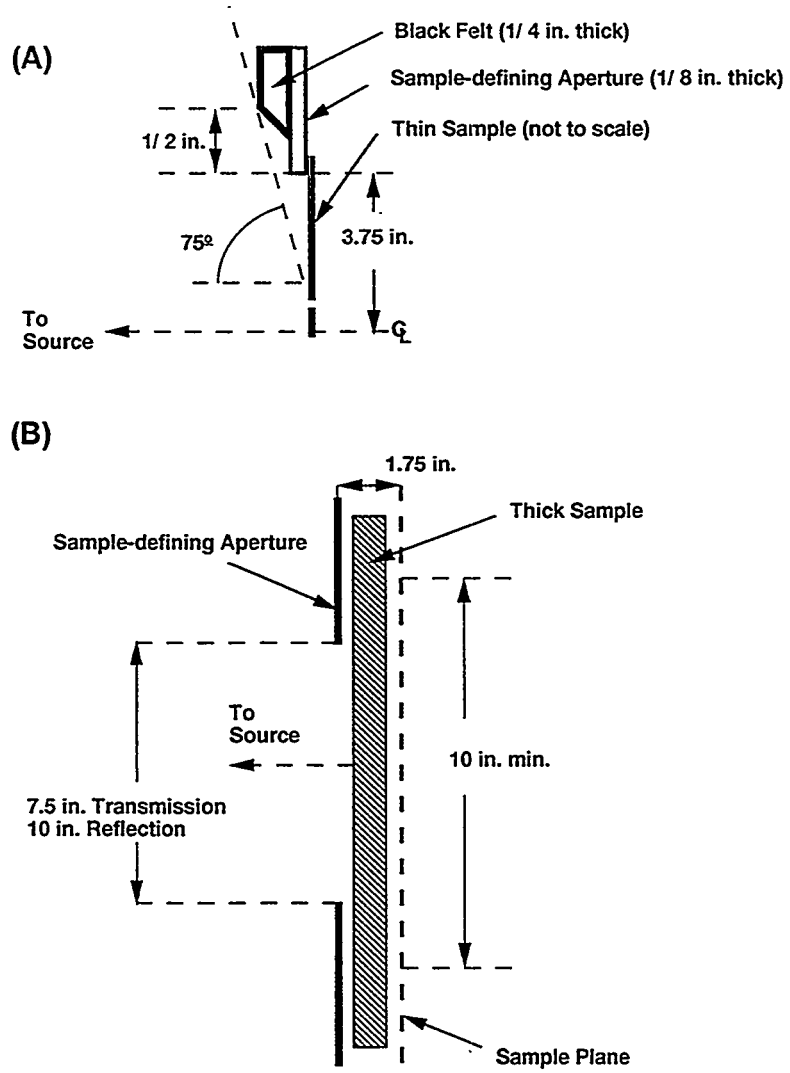

Fig. 7 Sample Measurement Geometries. (a) Thin sample. (b) Thick sample.

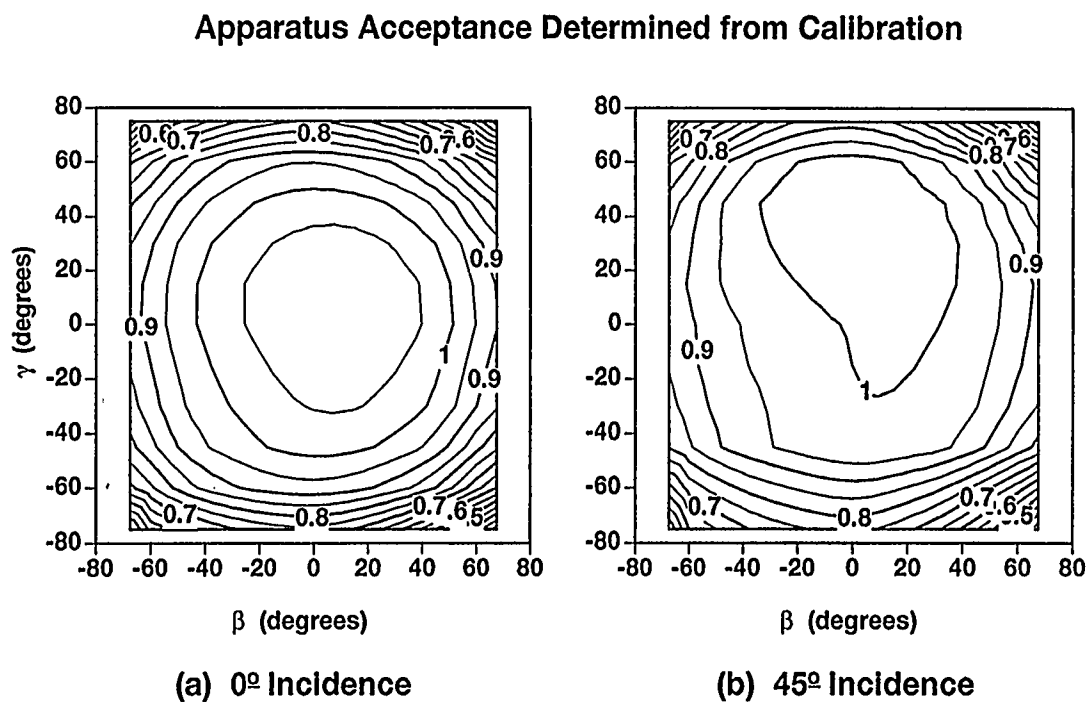

Fig. 8. Measured Apparatus Effective Acceptance for Two Incident Angles. Both at (a) normal incidence and (b) 45 degree incidence, the shape of the apparatus acceptance is flat for small outgoing angles and decreases for large outgoing angles as apertures hide parts of the sample edges from the detector. Small assymetries appear for non-normal incidence.

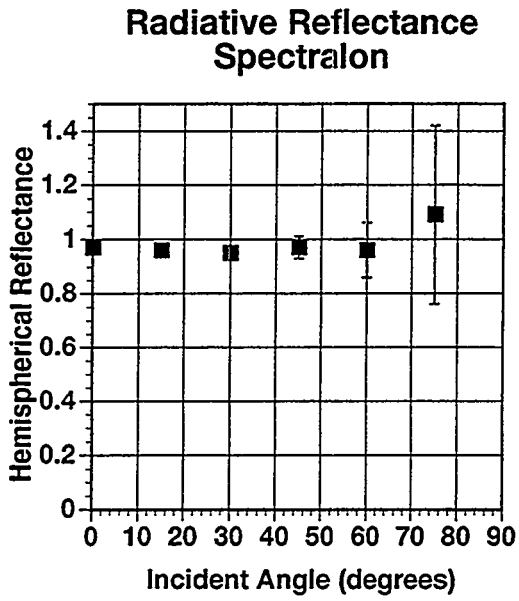

Fig. 9 Measured Hemispherical Reflectance of Spectralon® Calibration Sample. Data measured with the radiometric sensor was used in the determination.

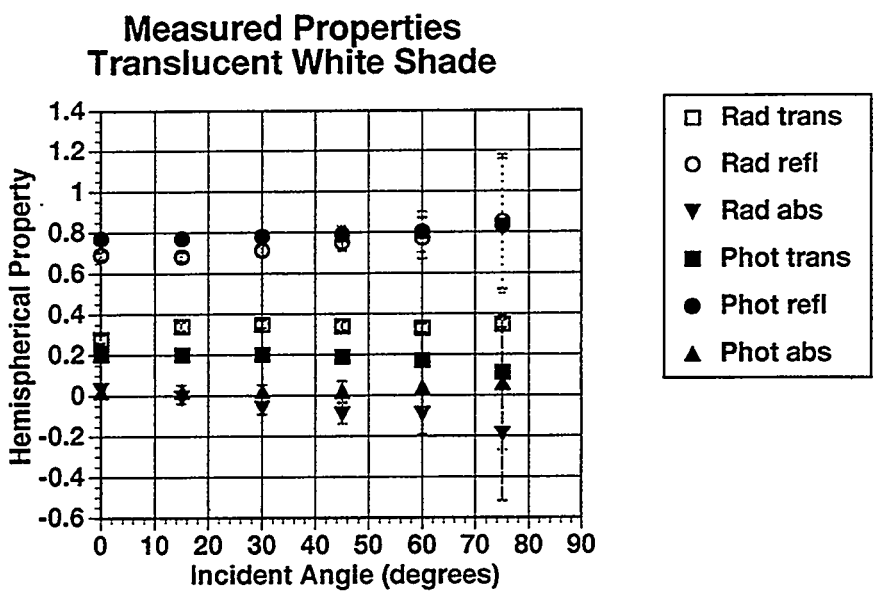

Fig. 10 Measured Directional-Hemispherical Properties of a Commercially Purchased Translucent White Shade.

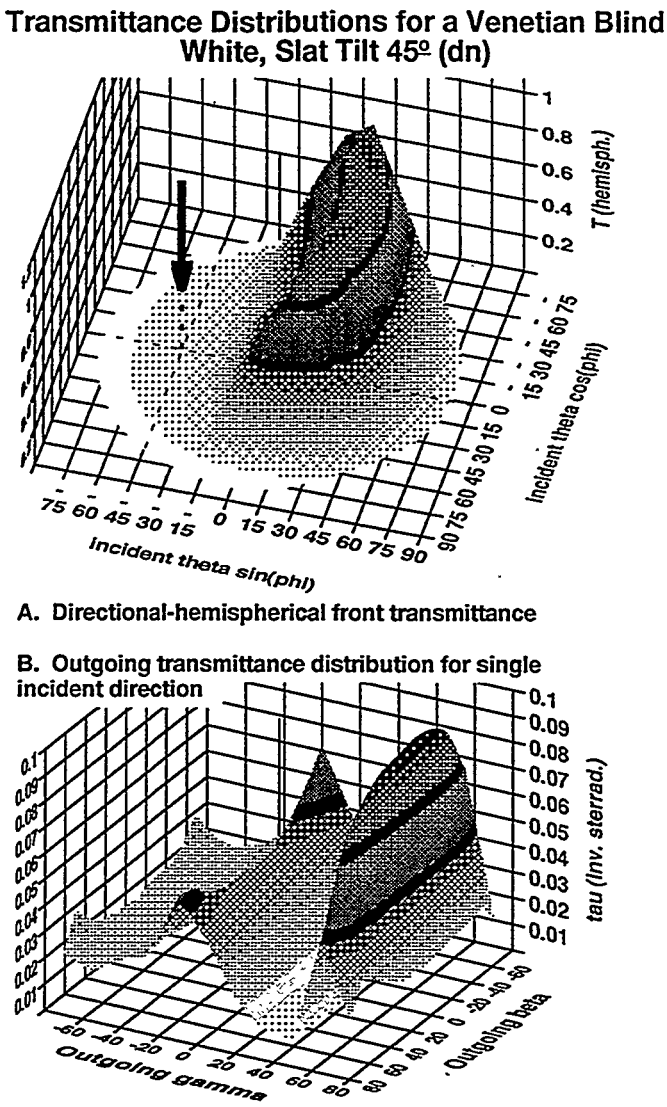

Fig. 11 Measured Front Transmittance Distributions for a White Venetian Blind. The slats of the blind were tilted "downwards" (i.e., in a direction that would tend to exclude direct sunlight) at an angle of 45°. The upper plot (A) gives the directional-hemispherical transmittance as a function of incident direction, while the lower plot (B) gives the output transmittance distribution for the particular incident direction indicated by the arrow in (A). The value of the directional-hemispherical transmittance at the point indicated by the arrow is obtained by integrating the output distribution (B). The incident direction angles are given in the sample coordinate system utilized in the layer calculation, while the outgoing angles displayed are those of the scanner measurement coordinate system, as explained in the text. For the incident direction in (A) the choice of x and y axes effectively yields a set of polar coordinates in the angles θ and ϕ. The azimuthal angle, ϕ, in the plane of the blind falls in the range $\pi \leq \phi \leq 2\pi$ because the incident direction is specified as the direction *of travel* of the incident rays, rather than the more usual definition as the direction *from* the window *to* the light source.

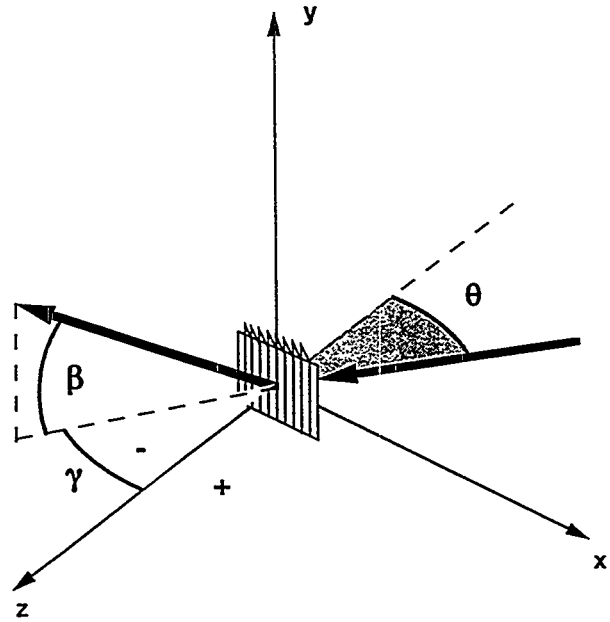

Fig. 12. The Measurement Configuration Illustrated in Fig. 11.

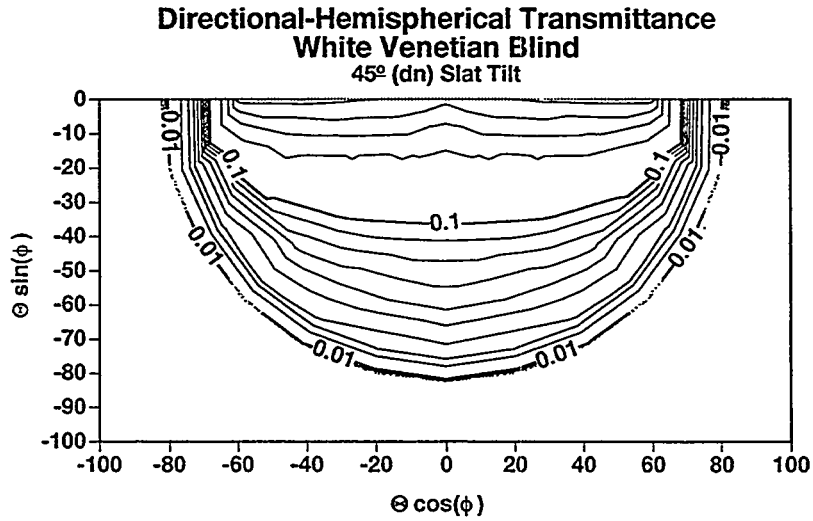

Fig. 13. A Contour-Plot Display of the Directional-Hemispherical Front Transmittance of a Venetian Blind for Downward-Going Incident Directions. A detail of the data from Fig. 11 (A) for downward-going incident directions. Contour intervals are logarithmic in transmittance. Low-angle, relatively high-transmittance data reflects the rectilinear geometry of the blind slats, while this geometric detail washes out in transmission at large outgoing angles due to the multiple diffuse reflections that produce this transmission.